



Article

Exploring Convective Drying Behavior of Hydroxide Sludges Through Micro-Drying Systems

Azeddine Fantasse, Sergio Luis Parra-Angarita, El Khadir Lakhal, Ali Idlimam, El Houssayne Bougayr and Angélique Léonard

Special Issue

New Approaches to Water Treatment: Challenges and Trends

Edited by

Dr. Luz Marina Ruíz and Prof. Dr. Miguel Ángel Gómez



Article

Exploring Convective Drying Behavior of Hydroxide Sludges Through Micro-Drying Systems

Azeddine Fantasse ^{1,*}, Sergio Luis Parra-Angarita ¹ , El Khadir Lakhal ², Ali Idlimam ³, El Houssayne Bougayr ⁴  and Angélique Léonard ¹ 

¹ Chemical Engineering Research Unit, PEPs, University of Liège, 4000 Liège, Belgium; slparra@uliege.be (S.L.P.-A.); a.leonard@uliege.be (A.L.)

² Laboratory of Fluid Mechanics and Energetics (LMFE), Faculty of Sciences Semlalia, Cadi Ayyad University, Marrakesh 40000, Morocco; lakhal@uca.ac.ma

³ Team of Solar Energy and Medicinal Plants (EESPAM), Teacher's Training College, Cadi Ayyad University, Marrakesh 40000, Morocco; aidlimam@gmail.com

⁴ Engineering & Applied Technologies Laboratory (LITA), Higher School of Technology—Beni Mellal, Sultan Moulay Slimane University, Beni-Mellal 23000, Morocco; bougayr@gmail.com

* Correspondence: azeddine.fantasse@doct.uliege.be

Abstract: The drying of hydroxide sludge is a critical step in its valorization process in drinking water treatment plants (WWTPs), due to the high energy requirements associated with this operation. This study investigates the convective drying behavior of hydroxide sludge using a convective micro-dryer, with air heated to temperatures between 70 °C and 110 °C, velocities ranging from 1 m/s to 3 m/s, and constant absolute humidity of 0.005 kg of water per kg of dry air. The process was continuously monitored through X-ray microtomography, allowing the nondestructive observation of external surface texture evolution, shrinkage, and crack formation. A significant shrinkage, with a volume reduction ranging from 30% to 45%, was observed as the moisture content decreased. The experimental data were used to develop a characteristic drying curve specific to hydroxide sludge, which remained consistent across different operational conditions. The results showed that increasing air temperature and velocity enhanced the drying flux and reduced drying time, while higher air humidity produced the opposite effect. Additionally, the crack formation observed towards the end of the drying process was associated with internal moisture transfer limitations. Effective diffusivity increased with air temperature, highlighting the significant impact of temperature on the activation energy of the drying process. These findings provide valuable insights for optimizing the energy efficiency of sludge-drying operations.

Keywords: hydroxide sludge; drying; effective diffusivity; shrinkage and cracks; X-ray microtomography



Academic Editors: Luz Marina Ruiz and Miguel Ángel Gómez

Received: 9 January 2025

Revised: 22 February 2025

Accepted: 26 February 2025

Published: 21 March 2025

Citation: Fantasse, A.; Parra-Angarita, S.L.; Lakhal, E.K.; Idlimam, A.; Bougayr, E.H.; Léonard, A. Exploring Convective Drying Behavior of Hydroxide Sludges Through Micro-Drying Systems. *Appl. Sci.* **2025**, *15*, 3470. <https://doi.org/10.3390/app15073470>

Copyright: © 2025 by the authors. Licensee MDPI, Basel, Switzerland. This article is an open access article distributed under the terms and conditions of the Creative Commons Attribution (CC BY) license (<https://creativecommons.org/licenses/by/4.0/>).

1. Introduction

The generation of sludge is an unavoidable consequence of operations at drinking water treatment plants (DWTPs). In Morocco, the estimated monthly production of sludge derived from potable water treatment reaches approximately 16,000 tons of dry matter (DM). Typically, around 30 g of sludge is produced per liter of water treated [1]. These sludges, commonly referred to as clarification or hydroxide sludges (HSs), are characterized by a low content of biodegradable organic matter and a poor-quality texture [2].

The HSs, which initially exhibit a semi-liquid or “soupy” consistency, undergo multiple treatment stages aimed at reducing the water content [3]. These stages involve

thickening and dewatering, typically achieved through the addition of substantial amounts of polyelectrolytes. The thickened HS, with a suspended solids concentration of approximately 30 g/L (DM), is further dewatered using sand and gravel filtration systems and subsequently dried through evaporation on drying beds. HSs must be either disposed of in regulated landfills or repurposed for other uses [4]. The duration of the drying cycle, which is highly dependent on climatic conditions, particularly precipitation and evaporation rates, typically ranges from 60 to 80 days [1].

The raw water processed during treatment typically contains varying concentrations of suspended solids, including materials such as marl and clay, which are prone to rapid sedimentation [5]. The recovery and storage of these suspended solids, however, present significant technical challenges. In accordance with regulatory frameworks, potable water sludges are generally classified as “non-hazardous” or “ordinary waste”. Nevertheless, the management of HSs has emerged as a critical priority due to the substantial rise in their production, driven by accelerated urbanization and increasingly stringent regulations governing their disposal [2].

Several technologies have been proposed for the treatment and valorization of HSs, with drying standing out as a key technique. This process not only aligns with sustainable development principles but also plays a crucial role in HS management by reducing the mass and volume of the material, consequently lowering costs related to storage, handling, and transportation [6].

The fundamental principle of thermal drying entails the application of energy to a solid–liquid mixture in order to remove the solvent contained within it [7]. The energy required for HS thermal drying can be transferred through mechanisms such as conduction, convection, or radiation. This thermal drying stage, which follows mechanical dewatering, provides significant advantages, particularly in terms of agricultural valorization and potential energy recovery [8]. The target dryness level during the drying process is determined by the specific application for which the HS is intended.

Drying operations provide several notable benefits. One of the primary advantages is the significant reduction in both volume and mass through water removal, which directly impacts costs associated with storage, transportation, and handling. Granulated sludges exhibit the added benefit of requiring minimal maintenance during storage. Drying allows HS to be used with minor processing in road filler, cement clinker, quarry reclamation material, landfill sealing, composting co-substrate, built material, among others [8]. The process also stabilizes HS by reducing the possibility of oxidation and fermentation in case of high organic content, mitigating odor, especially when the dryness level exceeds 90%. At such low moisture levels, the decreased water activity inhibits bacterial growth, thus enhancing stability. Moreover, drying contributes to the hygienization of the HS by effectively destroying pathogenic microorganisms when temperatures are sufficiently high (e.g., 30 min at 70 °C), which is in line with European regulatory directives. Finally, the HS undergoes a transformation from a pasty to a solid texture, facilitating its subsequent handling and spreading.

In contrast to previous studies, which mainly focus on conventional drying techniques or general sludge characterization, this work introduces a new approach by relying on X-ray microtomography for real-time, non-destructive monitoring of HS drying. This technique enables detailed analysis of shrinkage dynamics, crack formation, and the limits of internal moisture transfer, which have not been studied in depth to date. In addition, the development of a characteristic drying curve specific to HS, consistent under various operational conditions, provides a new predictive tool for optimizing energy efficiency in HS drying operations. These contributions make this study a valuable step towards improving HS management in drinking water treatment plants.

2. Materials and Methods

2.1. Sludge Samples

The sludge samples used in this research came from the Marrakech DWTP. In order to produce drinking water to supply the population of the city of Marrakech and surrounding centers, the plant has two well-differentiated treatment processes, that of the water treatment process and the sludge treatment process. The treatment of water in the plant follows a classic process, as shown in Figure 1, with the following succession of stages: screening, de-sludging, pre-chlorination, coagulation/flocculation, decantation, filtration, and post-chlorination. The reagents used to ensure the treatment are as follows: aluminum sulfate as the main coagulant, polyelectrolyte as a flocculation aid, and chlorine gas to ensure oxidation and disinfection.

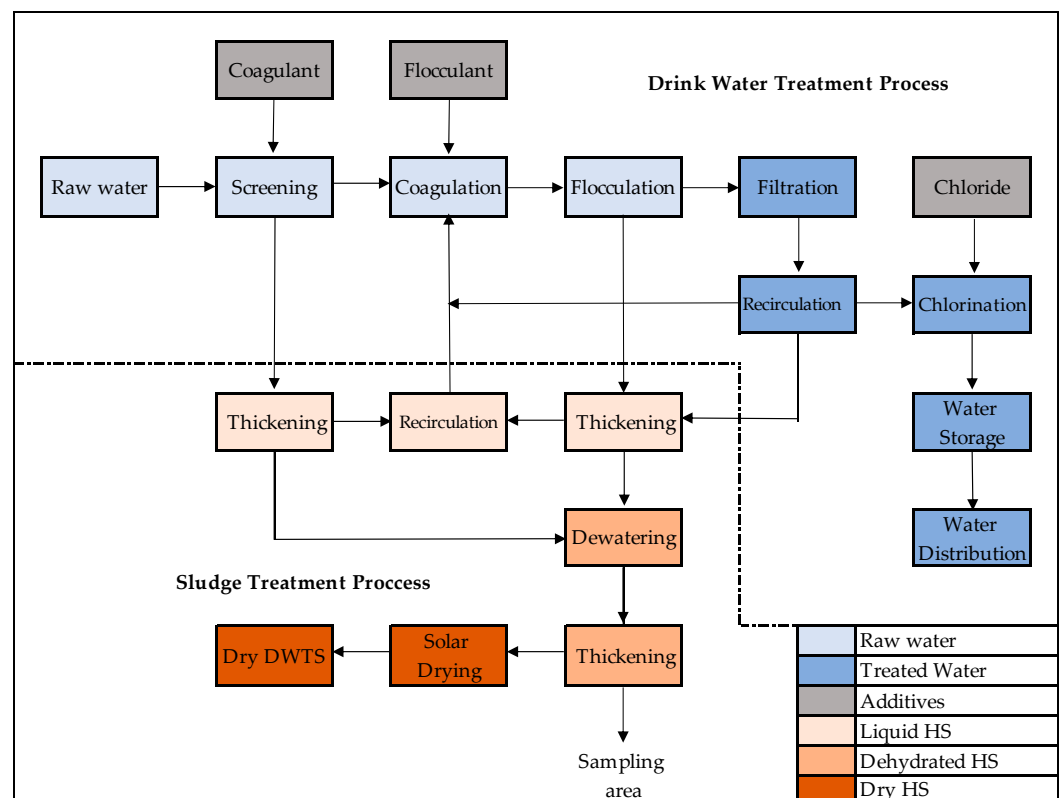


Figure 1. DWTS process plan.

The sludge treatment begins when the sediment streams from the primary and secondary treatments are thickened, followed by mechanical dehydration and a second thickening; finally, the sludge is solar-dried in large open pools. The samples were taken from the sludge's second thickening tank, as shown in Figure 1.

To define the chemical composition of drinking water treatment sludge (DWTS) and to monitor the effect of floods, which may occur during the rainy season, DWTS samples were taken during the wet season. After sampling, the samples were centrifuged and stored at 4 °C for the duration of the characterization period (4 weeks). The samples, initially containing 27% solids, underwent centrifugation for 13 min at a speed of $8000 \times g$ revolutions per minute (rpm), resulting in samples with 55% solid content on a wet basis [3].

The physical, chemical, and textural properties have been previously documented, published, and subjected to comprehensive analysis in a prior study [9].

2.2. Drying Tests

In this study, a full factorial design with two factors, each at three levels, was employed to evaluate the effects of temperature and air speed on the drying process. The key responses evaluated included the time required to reach 90% solid content, the average drying rate (or evaporation rate), the volume change (or shrinkage), and the critical moisture content. Detailed information regarding the factor levels, units, and response measurements is provided in Table 1. The experimental design results were analyzed using the Design Expert 13 software.

Table 1. Experimental design factors and responses.

Factors					
Variable	Abbreviation	Units	–	0	+
Temperature	T	°C	70	90	110
Air speed	V _a	m/s	1	2	3
Diameter	D	mm		12	
Height	H	mm		15	
Responses					
Drying time	Dt	Min			
Evaporation rate	Mv	kg _{water} /min			
Critical moisture	Xc	kg _{water} /Kg _{DS}			
Total shrinkage	%Sh	%Vo _{loss}			

The sludge samples were extruded and covered with a paraffin jacket (as shown in Figure 2) to make the drying and handling easier.

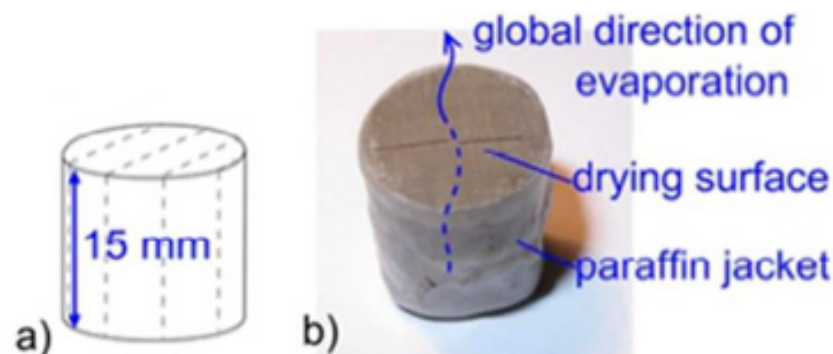


Figure 2. Sample geometry (a) and covering (b) [10].

The drying experiments were performed using a convective “micro-dryer” (Figure 3), specifically designed to process small, extruded sludge samples ranging in mass from 0.5 to 5 g. The micro-dryer operates under conventional convective drying conditions, controlled by key parameters such as relative humidity, temperature, and air velocity. Further technical details of the micro-dryer setup have been thoroughly described in a previous study [7]. The absolute humidity of the air was maintained at a constant value of 0.005 kg of water per kg of dry air.

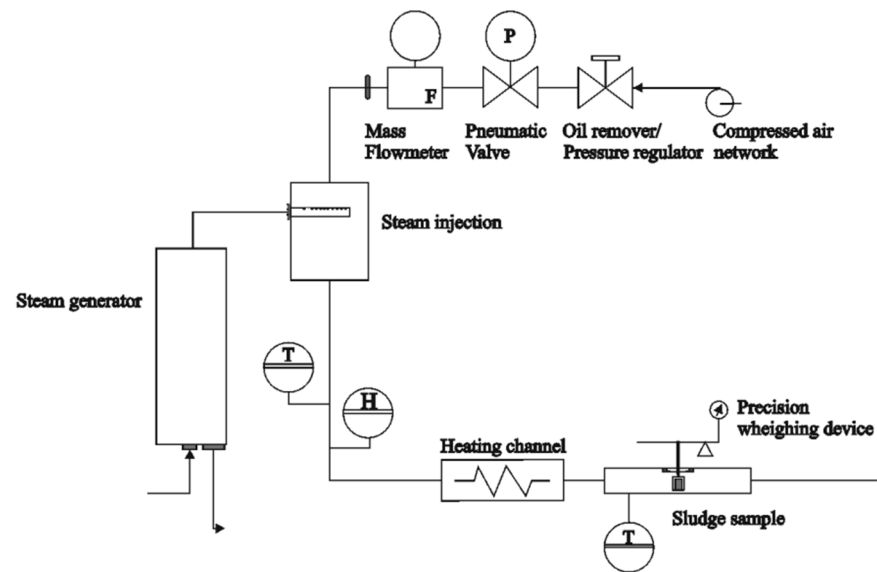


Figure 3. Micro-dryer tool [11].

During the experiments, the drying exchange surface and volume of sludge samples were measured through the drying (i.e., samples' shrinkage) using the methodology created by A. Léonard (2002) [7]. During the drying test, the sludge samples were removed from the dryer chamber and placed in the X-ray microtomographic device in order to obtain images of several cross-sections, then the samples were replaced in the micro-drier. The sequence was repeated about 10 times during the drying process. It has been verified that the drying interruptions do not exert any influence on the drying kinetics [12–14].

The X-ray microtomographic equipment employed in this study was a “Skyscan-1074 X-ray scanner”. Operating at 40 kV and 1 mA, the X-ray source is accompanied by a 2D detector comprising a 768×576 -pixel, 8-bit X-ray camera that generates images with a pixel size of $41 \mu\text{m}$.

The supplied software (Skyscan/NRecon) accompanying the machine was utilized for the image reconstruction processing. The quality of the resulting image is influenced by the quantity of acquired data, and its improvement is directly proportional to the number of projections captured. Subsequently, MATLAB software was employed for the analysis of the microtomography-derived images and their conversion into mathematical data suitable for generating the Krischer representation. Figure 4 shows, from left to right, the raw images obtained from tomography, a transverse cut obtained from Nrecon.

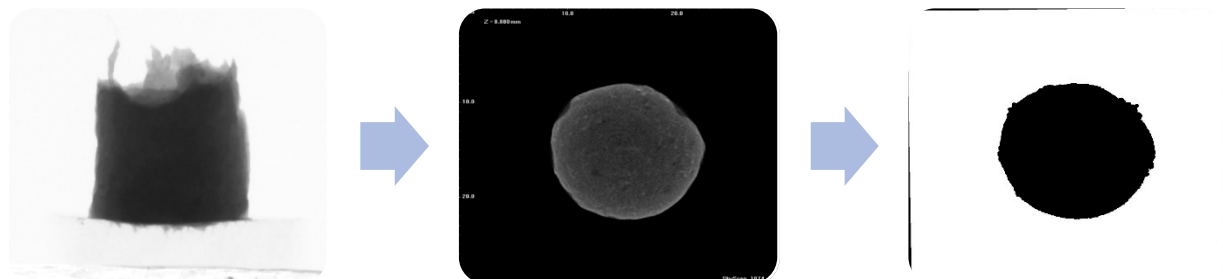


Figure 4. Images before and after processing.

During each interruption of the drying process, the average equivalent diameter (d_{eq} , mm) and average height (h , mm) were determined and utilized to calculate the surface area of the sample. In this study, the sludge samples were assumed to be perfect cylinders

with their entire surfaces in contact with the drying air. The obtained equations for each sample were used for the calculation of water flux and the plotting of the Krischer's curve.

2.3. Shrinkage Curves

The purpose is to analyze in more detail the transient response obtained under convective drying solicitation. A shrinkage curve illustrates the evolution of volume normalized by initial volume (V/V_0) as a function of water content on a dry basis. Most of the studies in the literature define shrinkage curves using calipers [7,15] by measuring displaced volume [7].

In the present work, shrinkage curves are obtained on the same principle as the external surface. For each interruption, the volume is calculated from the mean equivalent diameter and the mean height.

2.4. Effective Diffusivities

The diffusion coefficients can be determined using Fick's law, which describes moisture diffusion during the drying process. The general expression for Fick's law is as follows [16]:

$$X(t) = \frac{8}{\pi^2} \sum_{n=0}^{\infty} \frac{1}{(2n+1)^2} \exp\left(-\frac{(2n+1)^2 \pi^2 \text{Deff} \cdot t}{4L^2}\right) \quad (1)$$

For practical applications, this equation can be expressed in logarithmic form, as shown below [16]:

$$\text{Ln}(X) = \text{Ln}\left(\frac{8}{\pi^2}\right) - \left(\frac{\pi^2 \text{Deff}}{4L^2}\right)t \quad (2)$$

In this formulation:

- L represents the half-thickness of the material;
- X denotes the moisture ratio;
- Deff is the effective diffusion coefficient;
- t corresponds to the drying time.

The logarithmic transformation allows for the estimation of the effective diffusion coefficient as a function of time. The slope (m) of the linear relationship can be expressed as follows [16]:

$$m = \frac{\pi^2 \text{Deff}}{4L^2} \quad (3)$$

2.5. Activation Energy

The activation energy (E_a) is calculated using the Arrhenius equation [16]:

$$\text{Deff} = D_0 \exp\left(-\frac{E_a}{RT}\right) \quad (4)$$

In this equation:

- R is the universal gas constant ($\text{J/mol}\cdot\text{K}$);
- T is the absolute air temperature (K);
- E_a represents the activation energy (J/mol);
- D_0 is the pre-exponential factor in the Arrhenius model (m^2/s).

This approach facilitates the characterization of the temperature dependence of the diffusion process and provides insight into the energy required for moisture migration during drying.

3. Results and Discussion

3.1. Drying Kinetics

The drying process was controlled by repeatedly measuring the sample weight over a period of approximately 2 h, under different drying conditions. Figure 5 shows the variation of the sludge mass during the drying time at different temperatures for each air velocity studied. From the 3 graphics it's possible to say that higher temperatures have a bigger mass loss over the time, as expected. The drying time difference between the lowest and highest air speed is near to 100%; meaning that, sludge dried two time faster.

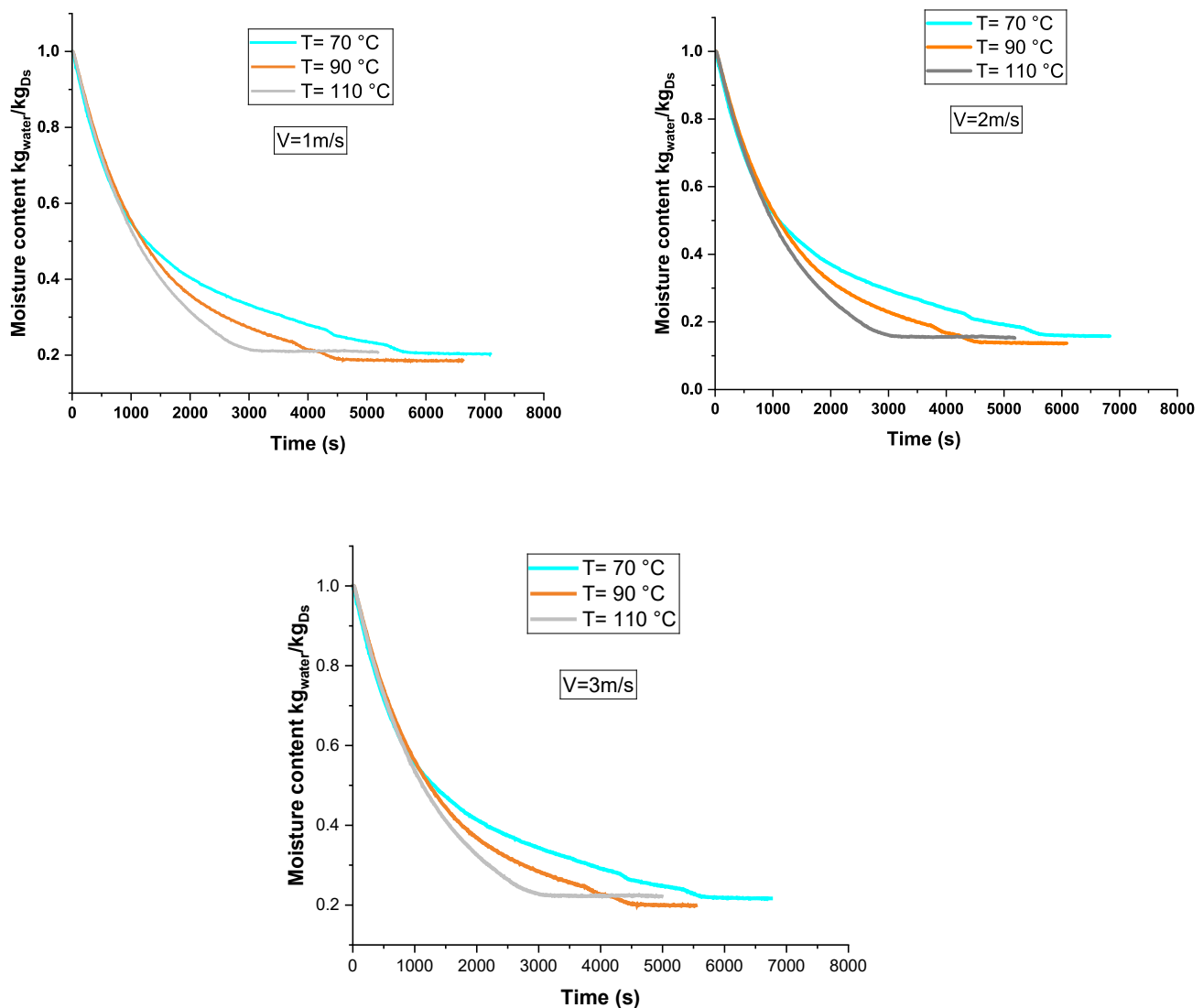


Figure 5. Moisture content versus time.

The mentioned above can be seen easily in Figure 5 which shows the moisture content versus time under varying temperature (70–110 °C) and air velocity (1–3 m/s). At higher temperature (e.g., 110 °C), moisture content decreases more rapidly over time due to the enhanced evaporation rate and increased internal moisture diffusion. The curves for lower temperatures (e.g., 70 °C) exhibit a slower decrease in moisture content, indicating a prolonged drying process.

Similarly, higher air velocities (e.g., 3 m/s) further accelerate the moisture removal by reducing the thickness of the boundary layer around the material and improving convective

mass transfer. Lower air velocities (e.g., 1 m/s) result in a slower drying process as the driving force for moisture evaporation is less effective.

Figure 6 shows the drying rate as a function of sample water content. As shown, a drying curve can be divided into three parts, a preliminary heating zone, where solid temperature and drying speed increase and gradually reach their maximum value, and a relatively narrow plateau, where solid temperature and drying rate are maintained at their maximum.

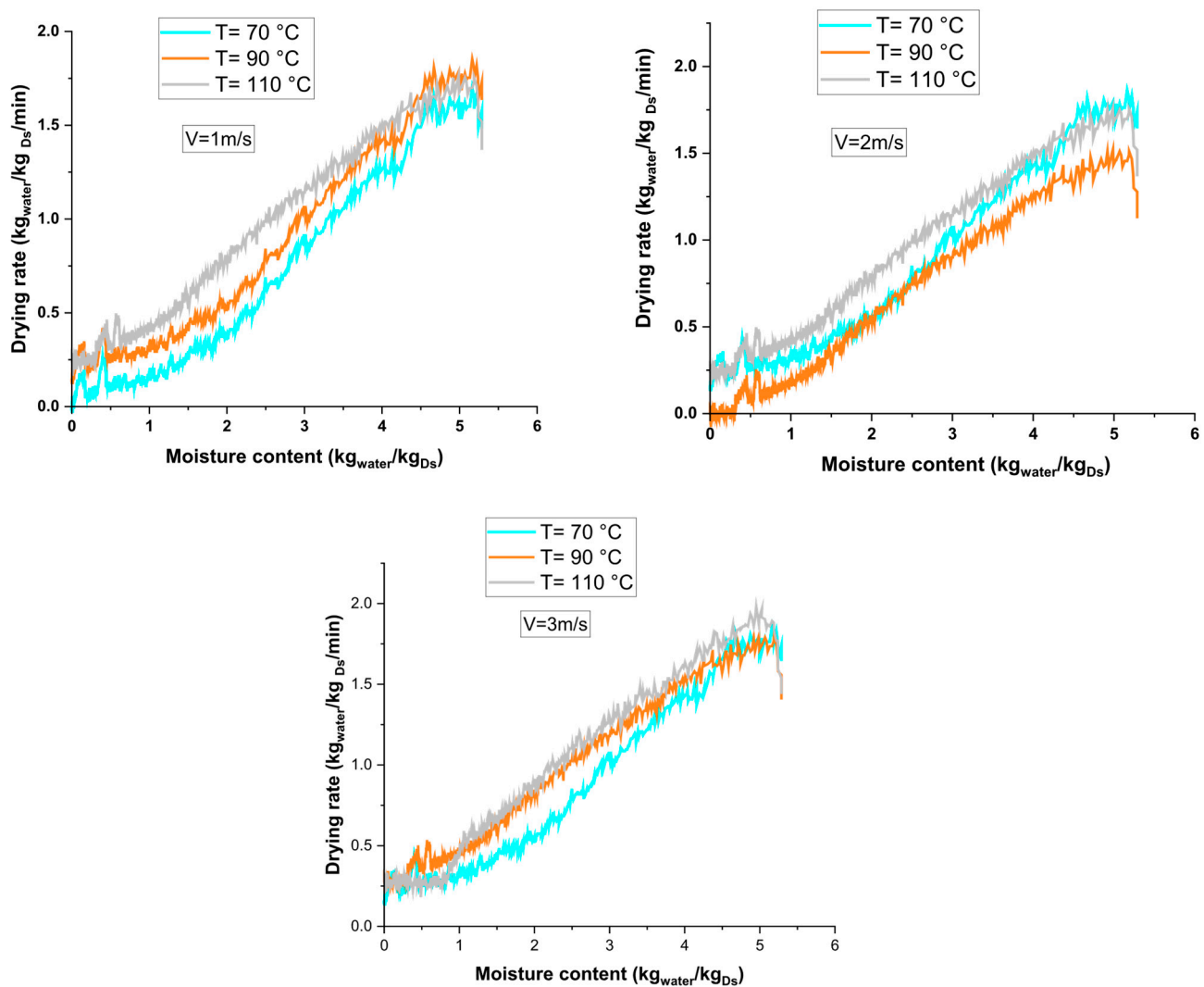


Figure 6. Drying rate versus moisture content.

The maximum mass flux and the drying rate both increase with the superficial air velocity, similarly to the mass transfer coefficient. Moisture is maintained keeping the driving force for mass transfer constant. However, the external solid surface begins to decrease due to shrinkage. As we can see in this figure, the moisture content of approximately 4.5 kg_{water}/kg_{Ds}, the mass flux of the drying rate is no longer constant, as illustrated in Figure 6. This implies that the driving force starts to decrease. Consequently, the moisture at the air–solid interface decreases due to limitations in internal heat and/or mass transfer. Shrinkage of the solid continues to affect the external surface. Therefore, the evolution of the drying rate is represented by the combined effects of shrinkage and limitations in internal transfer.

Figures 6 and 7 illustrate the impact of temperature and air velocity on the drying flux and rate. As shown, increasing the temperature enhances the drying flux and rate due to

a stronger vapor pressure gradient, which accelerates moisture evaporation and internal diffusion. Similarly, higher air velocity improves the removal of moisture from the surface by reducing the boundary layer resistance, maintaining a steady drying rate. These results highlight the combined effect of these parameters, where optimal temperature and velocity significantly improve drying efficiency.

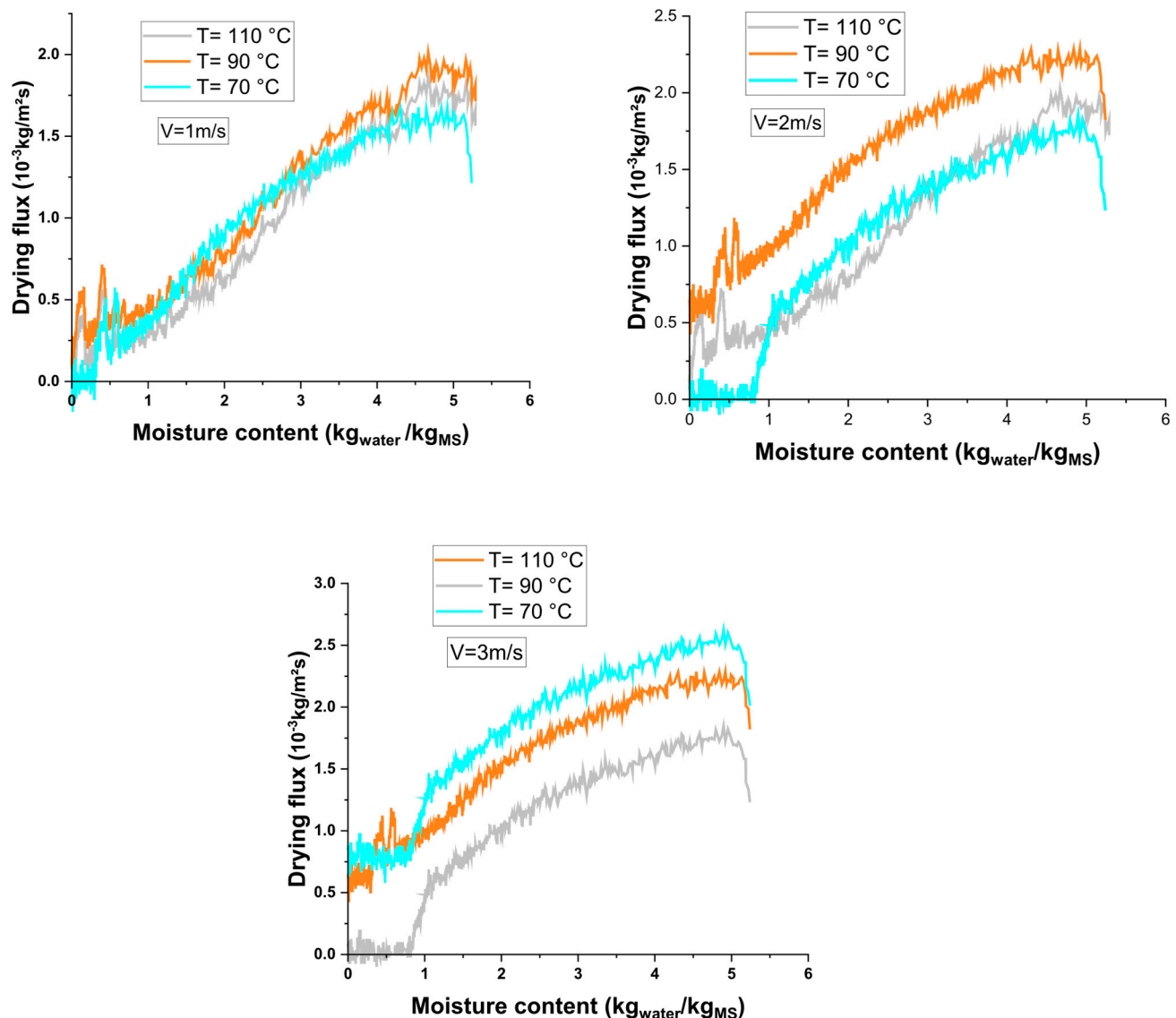


Figure 7. Drying flux versus moisture content.

The findings of this study demonstrate that increasing air temperature and velocity significantly enhances drying flux while reducing drying time, which aligns with the observations of [17]. However, while their study focused primarily on overall drying kinetics, it did not provide insights into the structural evolution of the sludge during drying. In contrast, our approach reveals a direct correlation between shrinkage dynamics and moisture content evolution, offering a more detailed mechanistic perspective on the drying process.

3.2. Volume and Shrinkage

The average height and surface area of the various cross-sections are used to calculate the volume of the sample at various time intervals, enabling a shrinkage curve to be determined. Figure 8 shows an example of a shrinkage curve, showing the normalized

volume (V/V_0) as a function of the water content of the sample, expressed on a dry basis (W/W_0) (kg water/kg solid). (V/V_0) represents the ratio of sample volume at a given point in the drying process to its initial volume.

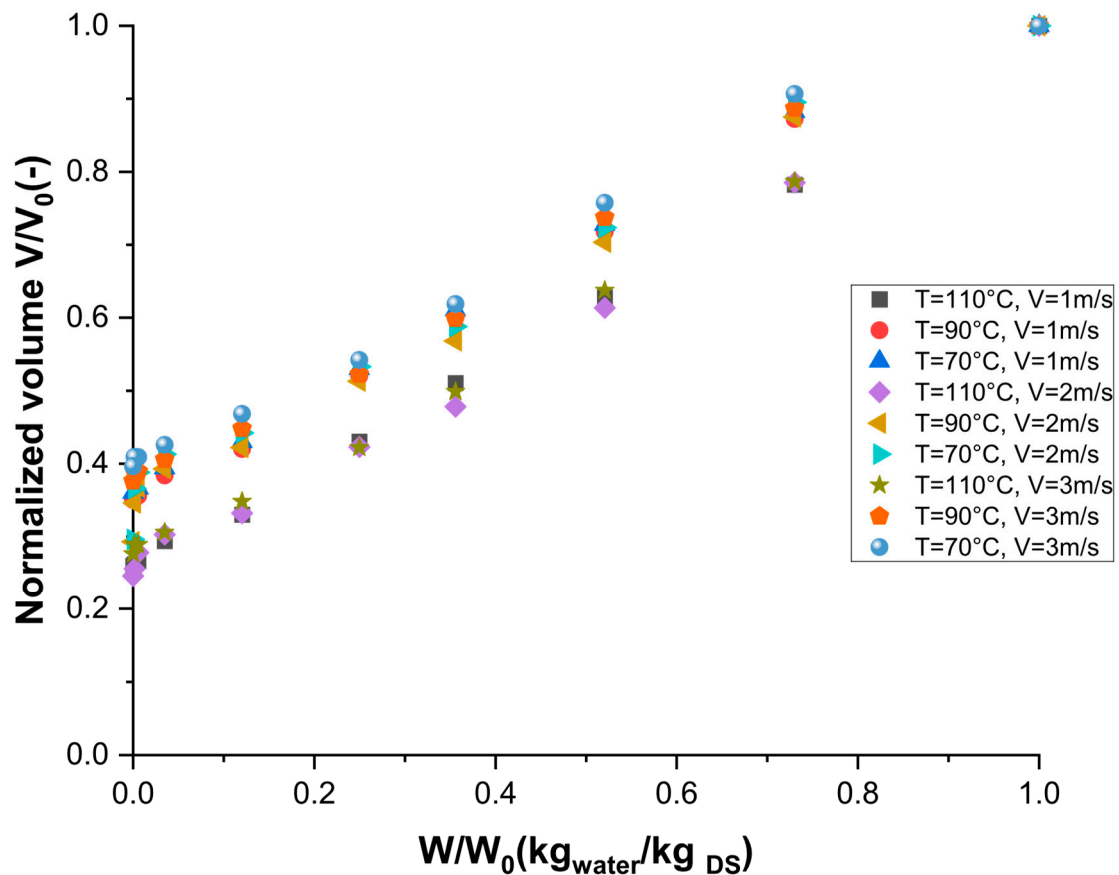

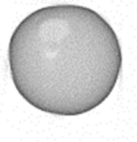
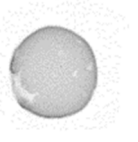
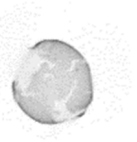
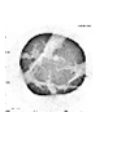
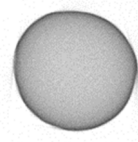
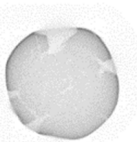
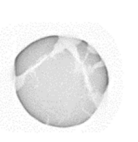
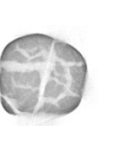
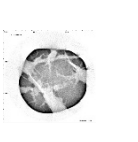
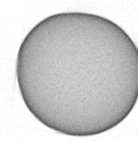
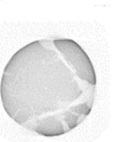
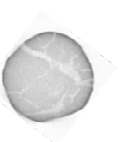
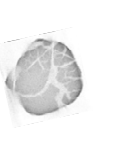



Figure 8. Normalized volume versus water content.

Figure 8 shows that shrinkage is almost linear with residual water content (W) up to a critical threshold (between 0 and 0.1 $\text{kg}_{\text{water}}/\text{kg}_{\text{DS}}$), for all three air velocities (1, 2, and 3 m/s). Volumetric shrinkage is considerable, with a maximum reduction in volume of around 80%. This volume reduction shows that shrinkage plays a crucial role in controlling the drying process.

In the previous part of this article, X-ray tomographic images shown in Table 2 were used to determine the external perimeter of the sampled cross-sections, from which the external surface area of the hydroxide sludge samples was calculated at a fixed temperature of 110 °C for three air-drying velocities. These cross-section images highlighted in Table 2 can also be used to analyze and monitor the evolution of internal texture during drying. As can be observed, the internal texture of the sludge remains unchanged for the air velocity of 1 m/s, that is, homogeneous (see the images corresponding to W equal to 5.3 and 3.7 $\text{kg}_{\text{water}}/\text{kg}_{\text{DS}}$). In contrast, more changes in texture are noticeable for the two air-drying velocities of 2 m/s and 3 m/s. The only visible change is the reduction in the size of the cross-sections. Some cracks appear and their significance increases as drying progresses (see the images corresponding to W equal to 1.5, 1.2, and 0.9 $\text{kg}_{\text{water}}/\text{kg}_{\text{DS}}$). It is therefore clear that crack formation is directly associated with the development of internal transfer limitations.

Table 2. Cross-sectional images of the three sludge samples following complete drying, acquired through X-ray microtomography.

Air Velocity	Sample Images During Drying at T = 110 °C				
1 m/s					
	W = 5.4	W = 3.7	W = 2.1	W = 1.5	W = 0
2 m/s					
	W = 5.3	W = 3.4	W = 1.9	W = 1.2	W = 0
3 m/s					
	W = 5.4	W = 3	W = 1.8	W = 0.9	W = 0

W in kg_{water}/kg_{DS}.

However, a key distinction in our findings is the characterization of crack formation at the final stages of drying, which has been briefly mentioned in the prior research [14,18] but not systematically analyzed. Our results indicate that the onset of cracks is intrinsically linked to internal moisture transfer limitations, a phenomenon that has critical implications for optimizing sludge drying processes and minimizing structural degradation.

If there are no significant internal transfer limitations, the moisture and temperature profiles inside the sample remain flat. But when internal transfer resistances develop, the mechanical stress induced by temperature and moisture distributions exceeds the maximum fracture strength of the material, and cracks progressively develop.

3.3. Drying Characteristic Curve of Hydroxide Sludge

Each drying parameter, such as duration and speed, varies according to the test conditions. Based on his experiments, [18] developed a drying rule to predict alternative dehydration curves under various conditions. The curve presented in Figure 9 establishes a dehydration rule derived from experiments, useful for predicting other dehydration curves under different air conditions, by knowing the initial water content and equilibrium water content (derived from sorption isotherms of hydroxide sludge) [1].

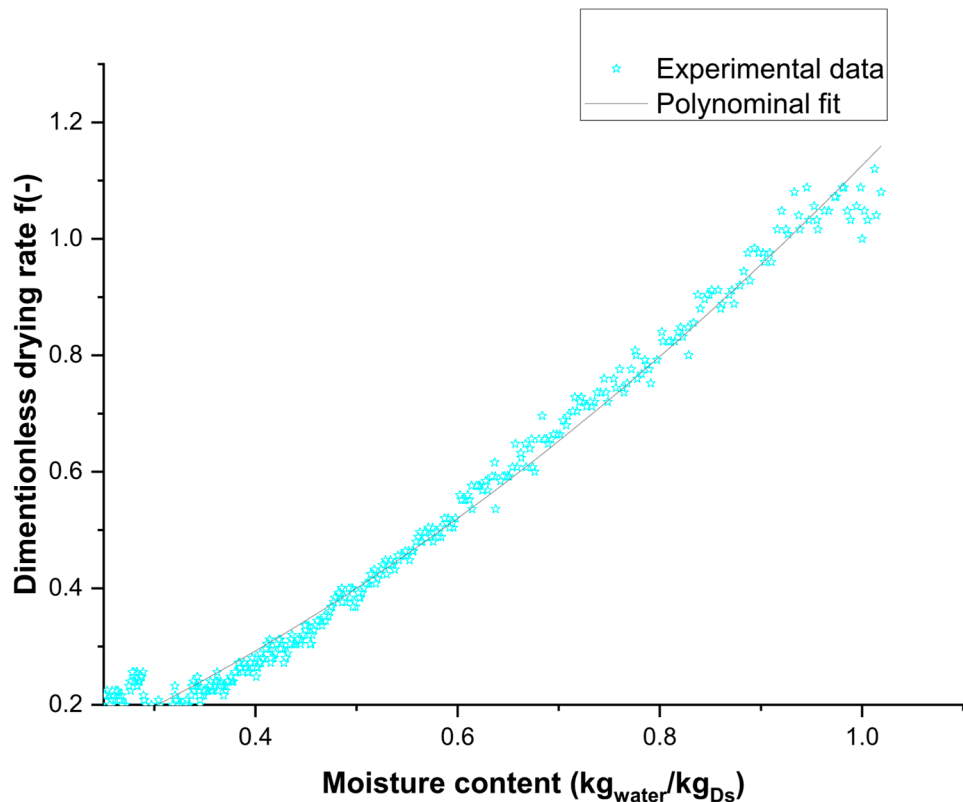


Figure 9. Drying characteristic curve.

To create this curve, test results under various air dehydration conditions are compiled into a single curve, called the CDC (characteristic dehydration curve), as demonstrated by the works of [19]. The variation in the moisture ratio against the dimensionless dehydration rate (f) is shown in Figure 9. The drying conditions significantly influence the rates of these curves. It was observed that the dehydration rate continuously decreases with decreasing water content. Furthermore, the dehydration rate increases with the air dehydration temperature, with the highest value recorded during tests at 110 °C. A linear function was found to be the most suitable for fitting the dimensionless experimental data of hydroxide sludge.

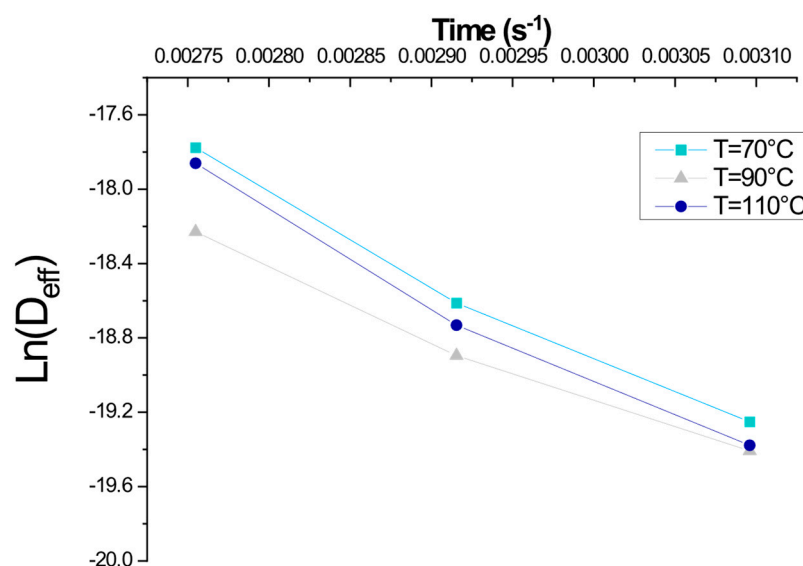
3.4. Activation Energy

The activation energy can be determined by plotting $\ln(D_{eff})$ as a function of $1/T$, which represents the influence of different drying air temperatures on the effective diffusivity. The effective moisture diffusivity D_{eff} was calculated using Equation (4) and is shown in Table 3. The effective diffusivity values of dried samples at 70–110 °C varied in the range of 3.73×10^{-9} and 1.75×10^{-8} m²/s. that D_{eff} values increased greatly with increasing temperature. Drying at 110 °C gave the highest D_{eff} values. Comparable findings have been reported in numerous studies. The effective moisture diffusivity D_{eff} values range from 8.486×10^{-10} to 4.386×10^{-9} m²/s for sewage sludge [20], 2.2×10^{-10} to 3.96×10^{-10} m²/s for paper mill sludge [21], and 1.91×10^{-8} to 9.12×10^{-8} m²/s for wastewater sewage sludge [22]. All studies found that increasing air temperature led to higher effective diffusivity values, while the effect of air velocity varied among materials. Furthermore, the effective diffusivity values obtained in our study are consistent with those reported by [18,23] who investigated convective drying under similar thermal conditions.

Table 3. Effective diffusivity and activation energy at different drying conditions for hydroxide sludge.

Air Velocity (m/s)	Temperature (°C)	D_{eff} (m^2s^{-1})	Ea (J/mol)	r
1	110	1.75×10^{-8}	32,547.04	0.996
	90	7.33×10^{-9}	32,213.81	0.985
	70	3.84×10^{-9}	31,879.23	0.897
2	110	1.21×10^{-8}	33,785.47	0.994
	90	6.22×10^{-9}	33,698.51	0.974
	70	3.73×10^{-9}	32,987.31	0.989
3	110	1.04×10^{-8}	33,457.21	0.975
	90	8.25×10^{-9}	32,496.93	0.996
	70	4.36×10^{-9}	31,548.63	0.938

This energy indicates the sensitivity of the reaction rate to temperature, as shown in Figure 10. The activation energy determined under varying air speed and temperature drying conditions ranged between 31.54 and 33.78 kJ/mol. A significant influence of air velocity and temperature on the activation energy is observed in several studies [16,20–22].

**Figure 10.** Arrhenius relationship between effective diffusivity and temperature.

4. Practical Applicability

The findings of this study hold significant potential for application in drinking water treatment plants (DWTPs) where sludge management remains a critical challenge due to the high energy demand of drying operations [24]. By identifying the key factors influencing the drying efficiency, such as temperature, air velocity, and shrinkage behavior, our study provides a framework for optimizing operational parameters to minimize energy consumption while ensuring effective sludge dehydration [25]. The discovery of a characteristic drying curve specific to hydroxide sludge offers a predictive tool that can be integrated into process modeling and real-time drying control systems, enabling more efficient resource utilization [3]. Additionally, insights into crack formation mechanisms can help improve the structural integrity of dried sludge, facilitating its handling, transport, and further valorization in industries such as construction or soil amendment [3].

5. Future Perspectives

Moving forward, several research avenues can be explored to expand upon our findings:

1. **Scaling Up the Study:** Future work should validate these results at an industrial scale, considering larger sludge volumes and different drying configurations to assess real-world applicability.
2. **Advanced Drying Optimization:** The integration of machine learning models and intelligent control systems could enhance real-time monitoring and adaptive process control, improving energy efficiency dynamically based on sludge properties.
3. **Valorization Pathways:** Investigating the potential reuse of dried hydroxide sludge in various industries, such as cement production, agriculture, or energy recovery, could further enhance sustainability in sludge management.
4. **Environmental Impact Assessment:** A Life Cycle Assessment (LCA) would provide a holistic evaluation of the environmental footprint of different drying strategies, supporting decision-making for more sustainable wastewater treatment processes.

By addressing these aspects, our study not only advances the scientific knowledge but also lays the groundwork for practical improvements in sludge management, with the ultimate goal of achieving more energy-efficient and sustainable drying operations in DWTPs.

6. Conclusions

In the context of sludge management in drinking water treatment plants, the energy-intensive process of drying holds significant importance. This study delves into the intricacies of sludge-drying behavior, aiming to improve its efficiency. A three-factor central composite design was implemented, encompassing temperature (ranging from 70 to 110 °C), air speed (varied between 1 and 3 m/s), and 12 and 15 mm of diameter and height, respectively. These parameters were investigated with respect to their impact on critical drying characteristics, including maximum drying flux, time required to achieve 95% dryness, final volume, and critical moisture content. The findings unveiled that elevated air temperature and velocity positively influenced maximum drying flux and final volume while reducing drying time. The observed volume reduction indicates that shrinkage is a key factor in governing the drying process. Analysis of the internal texture of the dried samples reveals the formation of cracks towards the end of the drying process. The onset of these cracks is clearly associated with the onset of internal transfer limitations; it is evident that the initiation of crack formation is intrinsically tied to the onset of internal transfer limitations. Conversely, air humidity exerts opposing effects. The impact of temperature on the overall behavior of the product throughout the process is evident, as water evaporation from the product increases with rising temperatures. A marked impact of temperature on activation energy is observed, with effective diffusivity showing a clear increase as dry air temperature rises, regardless of the air velocity. Notably, a paramount discovery emerged, namely, the drying curve's shape remains unaffected by these operational conditions, implying the presence of a unique characteristic curve specific to each type of sludge. This comprehensive investigation contributes valuable insights to enhance our understanding of hydroxide sludge drying behavior and its potential for energy-efficient optimization.

Author Contributions: A.F. contributed to the conceptualization, methodology, data collection and analysis, original draft preparation, review, editing, and supervision; S.L.P.-A. was involved in data collection and analysis, as well as drafting and reviewing the manuscript; E.K.L. participated in conceptualization, methodology, and provided supervisory editing; A.I. contributed to the methodology and supervisory editing; E.H.B. focused on data analysis, draft preparation, review, and supervisory editing; A.L. contributed extensively to conceptualization, methodology, data collection and analysis,

drafting, review, and supervision. All authors have read and agreed to the published version of the manuscript.

Funding: This work was supported by the Fund for Scientific Research (F.R.S.–FNRS) [T.0159.20-PDR].

Data Availability Statement: Data is contained within the article.

Acknowledgments: The authors acknowledge the support of the Chemical Engineering Halle personal in University of Liège. The authors acknowledge the FRS-FNRS, Fund for Scientific Research, for a Research Project, grant T.0159.20-PDR.

Conflicts of Interest: The authors declare that they have no competing interests related to this study.

References

1. Fantasse, A.; Lakhal, E.K.; Idlimam, A.; Kouhila, M.; Berroug, F.; El Haloui, Y. Management of Hydroxide Sludge Waste Using Hygroscopic Gravimetric Method and Physico-Chemical Characterization. *Mater. Today Proc.* **2020**, *27*, 3021–3027. [\[CrossRef\]](#)
2. Benlalla, A.; Elmoussaouiti, M.; Cherkaoui, M.; Ait Hsain, L.; Assafi, M. Characterization and Valorization of Drinking Water Sludges Applied to Agricultural Spreading. *J. Mater. Environ. Sci.* **2015**, *6*, 1692–1698.
3. Azeddine, F.; Khadir, L.E.; Ali, I.; Fatiha, B. Energy Efficiency of Drying Kinetics Process of Hydroxide Sludge Wastes in an Indirect Convection Solar Dryer. *J. Sol. Energy Eng.* **2021**, *143*, 041007. [\[CrossRef\]](#)
4. Chahid, L.; Yaacoubi, A.; Bacaoui, A.; Lakhal, E. Valorization of Drinking Water Treatment Sludge (DWTS): Characterization and Applications as Coagulant and Sorbent for Olive Mill Wastewater (OMW). *J. Mater. Environ. Sci.* **2015**, *6*, 2520–2533.
5. Azeddine, F.; Khadir, L.E.; Ali, I. Thermodynamic Analysis and Mathematic Modeling of Waste Sludge from Drinking Water Treatment Plants. *J. Ecol. Eng. JEE* **2022**, *23*, 140–149. [\[CrossRef\]](#)
6. Midilli, A.; Kucuk, H.; Yapar, Z. Drying Technology: An International Journal A NEW MODEL FOR SINGLE-LAYER DRYING. *Dry. Technol.* **2002**, *20*, 37–41. [\[CrossRef\]](#)
7. Léonard, A.; Blacher, S.; Marchot, P.; Pirard, J.P.; Crine, M. Drying Technology An International Journal Measurement of Shrinkage and Cracks Associated to Convective Drying of Soft Materials by X-Ray Microtomography. *Dry. Technol.* **2007**, *22*, 1695–1708. [\[CrossRef\]](#)
8. Hidalgo, A.M.; Murcia, M.D.; Gómez, M.; Gómez, E.; García-Izquierdo, C.; Solano, C. Possible Uses for Sludge from Drinking Water Treatment Plants. *J. Environ. Eng.* **2016**, *143*, 04016088. [\[CrossRef\]](#)
9. Fantasse, A.; Parra Angarita, S.; Léonard, A.; Lakhal, E.K.; Idlimam, A.; El Houssayne, B. Rheological Behavior and Characterization of Drinking Water Treatment Sludge from Morocco. *Clean. Technol.* **2023**, *5*, 259–274. [\[CrossRef\]](#)
10. Fraikin, L.; Herbreteau, B.; Salmon, T.; Nicol, F.; Crine, M.; Léonard, A. Use of an Experimental Design to Characterize the Convective Drying Behavior of Different Sludges. *Dry. Technol.* **2015**, *33*, 1302–1308. [\[CrossRef\]](#)
11. Leonard, A.; Blacher, S.; Marchot, P.; Crine, M. Use of X-Ray Microtomography to Follow the Convective Heat Drying of Wastewater Sludges. *Dry. Technol.* **2002**, *20*, 1053–1069. [\[CrossRef\]](#)
12. Pambou, Y.B.; Fraikin, L.; Salmon, T.; Crine, M.; Léonard, A. Sludge Dewatering and Drying: About the Difficulty of Making Experiments with a Non-Stabilized Material. *Desalination Water Treat.* **2016**, *57*, 13841–13856. [\[CrossRef\]](#)
13. Léonard, A.; Royer, S.; Blandin, G.; Salmon, T.; Fraikin, L.; Crine, M. Importance of Mixing Conditions during Sludge Liming Prior to Their Convective Drying. *Eur. Dry. Conf. Palma Spain* **2011**, 26–28.
14. Huron, Y.; Salmon, T.; Crine, M.; Blandin, G.; Léonard, A. Effect of Liming on the Convective Drying of Urban Residual Sludges. *Asia-Pac. J. Chem. Eng.* **2010**, *5*, 909–914. [\[CrossRef\]](#)
15. Bennamoun, L.; Crine, M.; Léonard, A. Convective Drying of Wastewater Sludge: Introduction of Shrinkage Effect in Mathematical Modeling. *Dry. Technol.* **2013**, *31*, 643–654. [\[CrossRef\]](#)
16. Bahammou, Y.; Tagnamas, Z.; Lamharrar, A.; Idlimam, A. Thin-Layer Solar Drying Characteristics of Moroccan Horehound Leaves (*Marrubium vulgare* L.) under Natural and Forced Convection Solar Drying. *Sol. Energy* **2019**, *188*, 958–969. [\[CrossRef\]](#)
17. Cox, A.E.; Camberato, J.J.; Smith, B.R. Phosphate Availability and Inorganic Transformation in an Alum Sludge-affected Soil. *J. Environ. Qual.* **1997**, *26*, 1393–1398. [\[CrossRef\]](#)
18. Rashvand, M.; Nadimi, M.; Paliwal, J.; Zhang, H.; Feyissa, A.H. Effect of Pulsed Electric Field on the Drying Kinetics of Apple Slices during Vacuum-Assisted Microwave Drying: Experimental, Mathematical and Computational Intelligence Approaches. *Appl. Sci.* **2024**, *14*, 7861. [\[CrossRef\]](#)
19. Borah, A.; Hazarika, K.; Khayer, S.M. Drying Kinetics of Whole and Sliced Turmeric Rhizomes (*Curcuma Longa* L.) in a Solar Conduction Dryer. *Inf. Process. Agric.* **2015**, *2*, 85–92. [\[CrossRef\]](#)
20. RuiXun, J.; Aimin, L.; Weiyun, W. Thin Layer Drying Characteristics and Kinetics Model of Dewatered Sludge. *China Environ. Sci.* **2009**, *29*, 22–25.

21. Kai, L.; Xiao-Qian, M.A.; Han-Min, X. Experiment and kinetics model analysis on thin layer drying of paper mill sludge. *J. Fuel Chem. Technol.* **2011**, *39*, 149–154.
22. Ameri, B.; Hanini, S.; Boumahdi, M. Influence of Drying Methods on the Thermodynamic Parameters, Effective Moisture Diffusion and Drying Rate of Wastewater Sewage Sludge. *Renew. Energy* **2020**, *147*, 1107–1119. [[CrossRef](#)]
23. Bougayr, E.H.; Lakhal, E.K.; Idlimam, A.; Fantasse, A.; Lamharrar, A.; Kouhila, M.; Abdenouri, N.; Berroug, F. Experimental Study and Modeling of Drying Kinetics and Evaluation of Thermal Diffusivity of Sewage Sludge. *Key Eng. Mater.* **2023**, *954*, 55–71. [[CrossRef](#)]
24. Azeddine, F.; El Khadir, L.; Ali, I. Experimental Investigation of Solar Greenhouse Drying of Hydroxide Sludge under Summer and Winter Climate. *Pol. J. Environ. Stud.* **2022**, *31*, 1025–1036. [[CrossRef](#)]
25. Bougayr, E.H.; Bahammou, Y.; Fantasse, A.; Lakhal, E.K.; Berroug, F.; Bouziane, A.; Idlimam, A. Stabilization of Sewage Sludge from North Moroccan Wastewater Treatment Plants Using Convective Indirect Solar Drying. *Ecol. Eng. Environ. Technol.* **2024**, *25*, 1–16. [[CrossRef](#)]

Disclaimer/Publisher’s Note: The statements, opinions and data contained in all publications are solely those of the individual author(s) and contributor(s) and not of MDPI and/or the editor(s). MDPI and/or the editor(s) disclaim responsibility for any injury to people or property resulting from any ideas, methods, instructions or products referred to in the content.